From quantum geometry to non-linear optics and gerbes: Recent advances in topological band theory

Tomáš Bzdušek ©*

Department of Physics, University of Zürich, Winterthurerstrasse 190, 8057 Zürich, Switzerland (Dated: November 26, 2025)

Topological principles constitute at present an integral component of condensed matter physics, permeating the modern characterization of electronic states while also guiding materials design. In this brief *Perspective*, I highlight three research threads in single-particle topological band theory that have recently gained momentum: (i) the rise of the *quantum geometric tensor*, whose components can at present be directly accessed with optical probes; (ii) the notions of *delicate and multigap topology*, which fall outside the scope of tenfold way and symmetry-based indicators yet leave robust physical fingerprints; and (iii) the consideration of *bundle gerbes*, which capture formerly overlooked higher-form topological aspects of energy bands. These distinct directions have been elegantly woven together: delicate and multigap topological insulators have peculiar features in quantum geometry that can be conveniently captured by bundle gerbes. This viewpoint exposes the recently identified quantization of a non-linear optical response and provides outlooks for its realization in crystalline solids.

I. QUANTUM GEOMETRIC TENSOR

While *Berry curvature* of Bloch states has become an established concept in condensed matter physics, entering the description of band topology [1] as well as semiclassical transport [2], recent years have witnessed a revival of interest in a further geometric aspect of energy bands: their *quantum* (or *Fubini-Study*) *metric*. Both quantities measure aspects of how the wave function changes when varying momentum. Specifically, Berry curvature quantifies the complex phase acquired by the state when it is evolved on a small closed loop in momentum space [Fig. 1(a)]; in contrast, quantum metric measures how quickly the state grows in orthogonal directions when departing away from an initial momentum [Fig. 1(b)].

Both Berry curvature [3] and quantum metric [4] can be extracted as components of a single mathematical object: the quantum geometric tensor (QGT). Assuming a single non-degenerate band $|u_n\rangle$ that depends on momentum k, QGT is defined as the gauge-invariant Hermitian matrix [5]

$$Q_{ab}^{n} = \langle \partial_a u_n | (\mathbf{1} - |u_n\rangle\langle u_n|) | \partial_b u_n \rangle, \tag{1}$$

where ∂_a indicates the derivative of the state with respect to the momentum component k_a . In two and three spatial dimensions (i.e., 2D and 3D), this amounts to a 2×2 resp. 3×3 matrix with complex entries. The QGT naturally decomposes in the following way [6]: its symmetric real part is the quantum metric (g_{ab}^n) and its antisymmetric imaginary part is proportional to the Berry curvature (F_{ab}^n) of the band $|u_n\rangle$. Although QGT has been recognized as a property of Bloch energy bands for decades, it has recently moved into the spotlight due to the relations of its components to optical responses (discussed below), to electron-phonon coupling [7], and to superfluid weight in flat-band superconductors [8, 9].

Berry curvature and quantum metric are not entirely independent. Notably in two dimensions, where Berry curvature has only a single component, this component is bounded

Further and less obvious constraints follow from considering optical responses, suggesting a deeper link between topology, quantum metric, and response theory. To illustrate a specific example, recall that the linear optical conductivity $[\sigma_{ab}(\omega)]$, with $a,b \in \{x,y,z\}$] can be related using the Kubo-Greenwood formula to an integral involving the inter-band Berry connection (also called *optical dipole*) $A_a^{nm} = \langle u_n | \partial_a u_m \rangle$, which encodes geometrical information about the optical transitions between the energy bands n and m [12]. A careful analysis of the introduced concepts has been employed to reveal a non-trivial bound on the possible size of a topological energy gap. Given a 2D insulating system, the resulting constraint is specified as follows: define (i) the optical weight W^0 as the integral over all frequencies of the real part of the optical conductivity $\text{Re}[\sigma_{xx}(\omega)]$, and (ii) let C be its Chern number. Then, the topological energy gap obeys [11]

$$\Delta \le \frac{4\hbar^2 W^0}{e^2 |C|}.\tag{2}$$

Equation (2) provides a clean and model-independent bound that relates experimentally accessible properties to a topological invariant. Following this line of reasoning [11, 13], it is further shown that integrals of quantum metric and of Berry curvature specify negative moments of the optical conductivity: up to an overall constant of $e^2/4\hbar$, the integral of $\text{Re}[\sigma_{aa}(\omega)]/2\omega$ is equal to the quantum weight K, while the integral of $\text{Im}[\sigma_{ab}(\omega)]/\omega$ amounts to the Chern number C.

Very recently, the relations between the components of QGT and optical responses have been turned around: the work of

in absolute value by the determinant of the quantum metric $(|F| \leq 2\sqrt{\det g})$ at every momentum k [10]. Correspondingly, a suitably defined (and non-quantized) integral of the quantum metric, called the *quantum weight* (K) [11], is bounded to be larger than the quantized integral of the Berry curvature (the *Chern number*, C).

^{*} tomas.bzdusek@uzh.ch

¹ Specifically, the computation of $\sigma_{ab}(\omega)$ corresponds to an integral involving $A_a^{nm}A_b^{nm}\equiv Q_{ab}^{nm}$ with n the occupied and m the unoccupied bands. This object relates back to quantum metric through $\sum_{m,m\neq n}Q_{ab}^{nm}=Q_{ab}^{n}$.

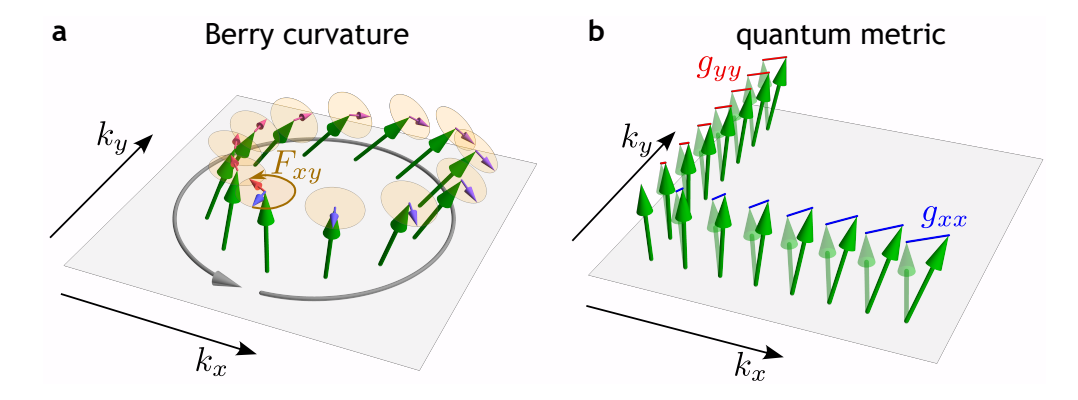


FIG. 1. Elements of the quantum geometric tensor. (a) Given an evolution of a Bloch state $|u_n\rangle$ (state vector, represented by green arrows) on a closed loop (circular gray arrow) inside the momentum space (plane of k_x and k_y), Berry curvature (F_{xy}) quantifies the complex phase (blue-to-red arrows within the attached disks) accumulated by the state. (b) Quantum metric (here only components g_{xx} and g_{yy} explicitly considered) quantifies the rate of change (blue and red line segments) of the Bloch state upon variation of the momentum coordinates.

Ref. 14 proposed a protocol for mapping QGT in the momentum space of 2D materials using momentum-resolved optical probes. Their starting point is that QGT of band $|u_n\rangle$ with energy E_n can be expanded using the full eigenspectrum of the Bloch Hamiltonian H as

$$Q_{ab}^{n} = \sum_{m \neq n} \frac{\langle u_n | \partial_a H | u_m \rangle \langle u_m | \partial_b H | u_n \rangle}{(E_m - E_n)^{\alpha}}$$
(3)

with exponent $\alpha = 2$. The key insight here is that the same expression with the exponent set to $\alpha = 1$, dubbed quasi-QGT (labeled q_{ab}^n), is conveniently accessed in experiments: its real part (the band Drude weight) can be estimated from band dispersion, accessible in conventional angle-resolved photoemission spectroscopy (ARPES), while its imaginary part (the orbital angular momentum) is extracted with circular-dichroism ARPES, in which one measures the difference in photoemitted electron intensity under using right-handed and left-handed circularly polarized light. Assuming an effective two-band approximation for the bands nearest to the Fermi level, the two tensors are related by simple rescaling $Q_{ab}^n=q_{ab}^n/\Delta E$, with the k-dependent energy gap ΔE readable from ARPES. The authors successfully illustrated their protocol with an application to the quasi-two-dimensional kagome material CoSn. The outlined experimental protocol was further advanced with the subsequent work of Ref. 15, which extracted the quantum metric tensor of the valence band of black phosphorus without resorting to the auxiliary quasi-QGT. Such a simplification was achieved by reconstructing the pseudospin texture by means of polarization-resolved ARPES measurements.

The relevance of QGT to optics does not terminate with linear (first-order) responses; rather, it extends to non-linear (higher-order) responses as well. In such cases, the conductivity becomes a higher-rank tensor, which encodes the current through $j_a \propto \sigma_{abc...} E^b E^c \cdots$, where the coefficients $\sigma_{abc...}$ are expressed as combinations of Berry dipoles A_a^{nm} and their

derivatives [12, 16, 17]. Notably, recent reformulation of certain second-order responses has revealed previously unrecognized *topological* aspects of band theory in three dimensions. To illuminate this hidden topology, it is valuable to briefly turn attention to the study of few-band toy models with certain unstable topological invariants.

II. DELICATE AND MULTIGAP TOPOLOGY

The 'stability' of a topological invariant means that it (i) can be defined in models with an arbitrarily large number of energy bands and (ii) cannot be trivialized through the addition of a trivial band (specifically: of an atomic limit) to either the occupied or the unoccupied sector [18, 19]. Stable topological invariants have been extensively classified across a broad range of symmetry settings (including Altland-Zirnbauer symmetry classes [20], various spatial dimensions, and space groups) with the language of symmetry-based indicators [21, 22] and elementary band representations [23] providing particularly valuable insights for first-principles calculations and materials design. (So-called *fragile topology* [24] corresponds to an intermediate scenario where the topological obstruction can be removed by including a trivial band to the occupied—but not by adding it to the unoccupied—part of the spectrum.)

Nevertheless, there are instances of refined topological invariants that apply only to models with a small total number of energy bands (*delicate* topology) or to models where the bands are partitioned by more than one energy gap (*multigap* topology). A paradigm example of delicate topology is the Hopf insulator [25]: a two-band model of a three-dimensional magnetic topological insulator that long resisted integration into a broader classification principle. Its topological invariant

² In this expression, various choices of the frequency arguments and spatial

indices for the current and electric fields are possible, depending on the physical mechanism and type of response (e.g., shift current, injection current, second-harmonic generation, jerk response) that one chooses to investigate.

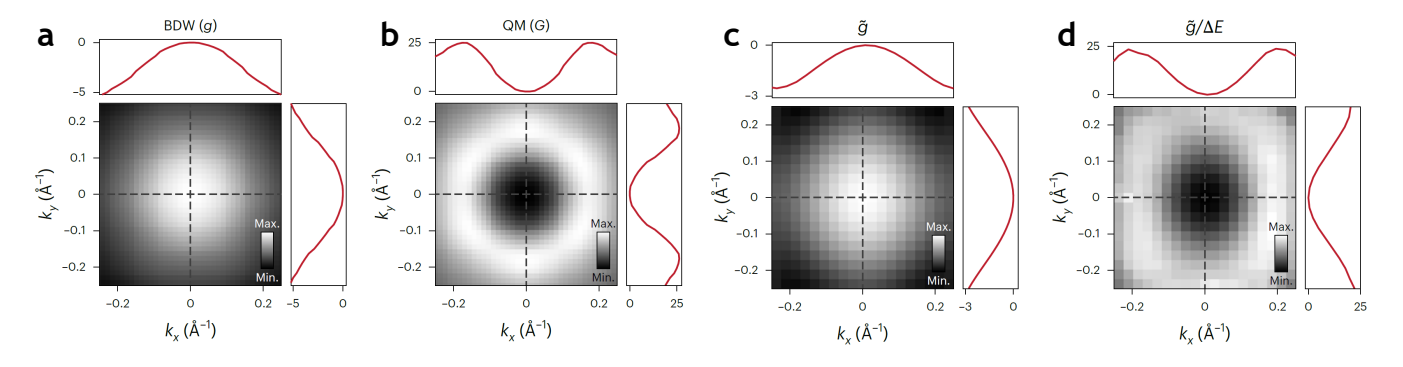


FIG. 2. Accessing the quantum geometric tensor. (a,b) Theoretical value of the band Drude weight and quantum metric in kagome material CoSn, and (c,d) their experimental estimates obtained through optical probes. (Image source: Ref. 14).

(the *Hopf invariant*) $h \in \mathbb{Z}$ is expressed elegantly as the integral of $A \cdot F$, i.e., of the dot product of the Berry connection and Berry curvature of the occupied band. However, the quantization of this integral is ensured only in strictly two-band models, indicating the loss of the Hopf topology in models involving three or more energy bands.

Multigap topology [Fig. 3(a-c)] got onto the scene with the discovery of non-Abelian braiding of band degeneracies in the momentum space of spinless PT-symmetric materials [26], i.e., those that exhibit combined space-time-inversion symmetry and negligible spin-orbit coupling. Specifically, while Dirac points in 2D band structures (such as that of graphene) carry a non-trivial value of a \mathbb{Z}_2 invariant (namely, a quantized Berry phase), whether a pair of Dirac points actually annihilate upon collision or not is dictated by their braiding around Dirac points in adjacent energy gaps. This reciprocal braiding of Dirac points in momentum space [27], experimentally demonstrated with acoustic meta-materials [28], is captured by assigning each Dirac point a non-Abelian invariant with values in the algebra of Pauli operators $\{\pm 1, \pm i\tau_x, \pm i\tau_y, \pm i\tau_y\}$: Dirac points in one energy gap carry 'charge' $\pm i\tau_x$ while those in an adjacent energy gap carry 'charge' $\pm i\tau_y$. The non-trivial braiding follows from the non-commutativity $\tau_x \tau_y = -\tau_y \tau_x$.

Abundant examples of unstable invariants have been characterized over the past five years. In few-band systems with mirror symmetry, given certain condition on mirror eigenvalues of the energy bands, returning Thouless pump RTP $\in \mathbb{Z}$ invariant can be defined [29], which corresponds to a quantized Chern number on half of the Brillouin zone (which is reverted on the complementary half). Furthermore, the Hopf invariant was found to extend to models with arbitrarily many bands as long as these are all non-degenerate throughout the 3D momentum space [30]. Crucially, spinless PT-symmetric systems turned out to be a particularly fertile ground for delicate and multigap topology. Beyond the already introduced non-Abelian invariant, any pair of energy bands in 2D can carry an *Euler class* $e \in \mathbb{Z}$ [27]. Non-zero values of e lead to fingerprints in QGT [31] and imply that the bands must be tied together with a minimum of 2|e| Dirac points. Further topological measures (real Hopf invariants, Pontryagin invariants, and isoclinic winding numbers) were introduced for collections of bands in spinless PT-symmetric models in 3D [32–34].

While such unstable topological models appear to be rather remote from applications to realistic crystalline solids, valuable insights have been gained by considering their non-linear optical properties. In particular, the shift current [Fig. 4(a)] constitutes a dc-response of non-centrosymmetric crystals to an ac-field of the form

$$j_a(0) = \sigma_{abc}^{\text{shift}}(\omega) E_b(-\omega) E_c(\omega). \tag{4}$$

It was reported [35] that models with non-trivial RTP admit a quantized contribution to the integral $\int d\omega \, \sigma_{xyy}^{\rm shift}(\omega)$ for a suitable orientation of the axes x and y. Furthermore, the integrated circular shift photoconductivity in three dimensions is quantized if any of the broad range of unstable invariants in spinless-PT-symmetric setups in 3D acquires a non-trivial value [36]. Remarkably, the mathematical descriptions developed in this context, phrased in terms of higher-form topological structures, provide hints for transferring these quantization results towards realistic materials, as described further below.

Two points concerning Eq. (4) merit clarification. First, the shift current in real materials includes multiple contributions [Fig. 4(b)]; namely, those induced by interband electronhole excitations via absorption of photons (shift_{exc.}), those induced by intraband relaxation via scattering with phonons and impurities (shift_{intra.}), and those induced by recombination of electron-hole pairs (shift_{rec.}) [37]. The reported quantized contribution relates solely to the 'excitation' part of the shift current. Whether this contribution dominates the nonlinear response depends on the specific material. Second, noncentrosymmetric crystals admit asymmetric excitation and scattering rates, enabling a further contribution to the dc-response called the ballistic current [38]. In the subsequent text, we simplify the discussion by focusing solely on the excitation part of the shift current, which has been reported to possess a topological character.

Before delving into the higher-form topological structures at play, let me also mention in passing two additional idiosyncrasies of delicate and multigap topology. First, they provide a novel paradigm for boundary anomalies. Recall that in conventional topological insulators one encounters 'topologically interesting' energy bands (e.g., ones carrying Chern number $\pm C$) that reside in the same physical space but are separated by an energy gap into the occupied and the unoccupied sec-

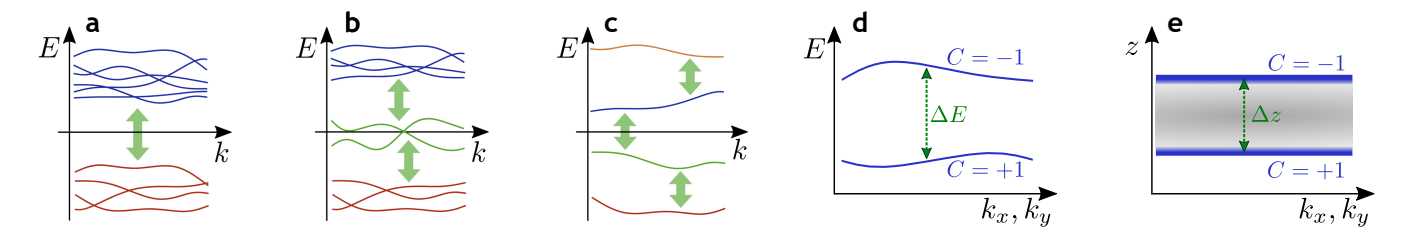


FIG. 3. Multigap and delicate topological insulators. (a) Conventionally, topological invariants are based on partitioning of the energy bands with a single energy gap determined by the Fermi level. (b,c) Recently, partitioning of energy bands by multiple gaps led to valuable insights into topological invariants and non-linear optical responses. Alternatively, if a topological invariant persists only for a small total number of energy bands, the topology is described as delicate. (d) Chern insulator in two dimensions exhibits energy bands characterized by opposite Chern numbers $\pm C$ which reside in the same physical space but are separated by an energy gap (ΔE). (e) In constrast, Hopf insulator in a three-dimensional slab exhibits surface features with opposite Chern numbers $\pm C$ that are physically separated by the system size (Δz).

tor [Fig. 3(d)]. In contrast, it is found that certain unstable topological models (including the Hopf insulator) in slab geometry exhibit analogous topologically interesting bands that are instead physically separated to reside on the top vs. the bottom surface of the slab [Fig. 3(e)] (while potentially being degenerate in energy) [39]. The second notable aspect is related to the previous one and concerns localization on disorder. Strong disorder in a Hopf insulator can generate a system in which all bulk eigenstates are localized at every filling, yet the phase is topologically nontrivial and enforces delocalized boundary transport with a quantized boundary Hall conductance enabled by the surface Chern number. Generalizing this phenomenology to higher dimensions and other Altland-Zirnbauer symmetry classes has very recently grown into the broader notion of *ultra-localized topological insulators* [40].

III. HIGHER-FORM TOPOLOGICAL STRUCTURES

To introduce the higher-form topology lurking behind the quantized contributions to non-linear optical responses, it is insightful to review the key mathematical objects in the context of 'Berryology' [top row of Fig. 5(a)] [42]. The determination of Berry curvature can be understood as a three-step process: first, find Bloch states $|u_n(k)\rangle$ in a smooth gauge in some region of the momentum space; second, compute the Berry connection $A_a^n=i\langle u_n|\partial_a u_n\rangle$ using the derivatives of the state; and third, compute the Berry curvature

$$F_{ab}^{n} = \partial_a A_b^n - \partial_b A_a^n \tag{5}$$

as an antisymmetrized derivative of the connection. If a gauge transformation $|u_n(k)\rangle\mapsto \mathrm{e}^{i\chi(k)}\,|u_n(k)\rangle$ is applied to the Bloch states, the Berry connection is altered, yet the Berry curvature remains unchanged. This is mathematically equivalent to the way the scalar and the vector potential in electromagnetism are changed by gauge transformations while the electric and magnetic fields remain invariant.

Here is how the same steps are presented in mathematical literature: The continuous association of momenta k to Bloch states $|u_n(k)\rangle$ is called a *vector bundle*, since one assigns a state vector (in the Hilbert space \mathscr{H}) to each momentum k. The notions of connection and curvature can be defined generally

for any vector bundle; for example, considering vectors tangent to a two-dimensional surface results in the usual geometric (i.e., Gaussian) curvature of the surface. The (anti-)symmetrization of the derivatives in Eq. (5) is important: it ensures that all the constructed objects are differential forms, whose integrals obey variants of Stokes' theorem [43]. Specifically, the Berry connection is described as a 1-form because it involves a single derivative, while the Berry curvature constitutes a 2-form due to the involvement of two derivatives.

The key idea behind *higher-form topology* is to find analogous mathematical objects where all the indices are increased by one [bottom row of Fig. 5(a)]. In other words: is it possible to construct a 'higher-form connection' (which involves two derivatives and that changes under gauge transformations) whose derivative gives a 'higher-form curvature' (which involves three derivatives and that is gauge-invariant)? The answer is affirmative, with the sought objects appearing in the integrated circular shift photoconductivity [34] (specifically, as alluded earlier, in the 'excitation' contribution to the shift current). The final expression (modulo unspecified coefficients and minus symmetrization over indices) takes the form [44]

$$\int d\omega \,\sigma_{abc}^{\text{shift,C}}(\omega) \propto \int_{\text{BZ}} d^3k \sum_{n \in \text{occ.}} \sum_{m \in \text{unocc.}} \mathcal{H}_{abc}^{nm} \qquad (6)$$

with the summations taken over all occupied and unoccupied bands. While the object \mathcal{H}^{nm}_{abc} on the right-hand side was originally formulated in the QGT context in terms of derivatives of the interband Berry connection [12], here I follow the more recent description in terms of bundle gerbes and tensor connections [44]—concepts borrowed from the string theory literature [45]. For simplicity, I will focus on spinless PT-symmetric models. Because a bulk shift current generally requires broken inversion, the condition "PT present with P broken" implies T is broken (for example, by antiferromagnetic order) while the combined PT symmetry remains intact.

One mathematically clean way³ of introducing bundle gerbes relates to properly generalizing the notion of gauge

³ The following two paragraphs (including Fig. 6) are aimed at specialists and rather technical in comparison with the rest of the text. They can be skipped without impacting the logic of the subsequent discussion. To achieve brevity, I employ the exterior derivative *d* in the equations involved here.

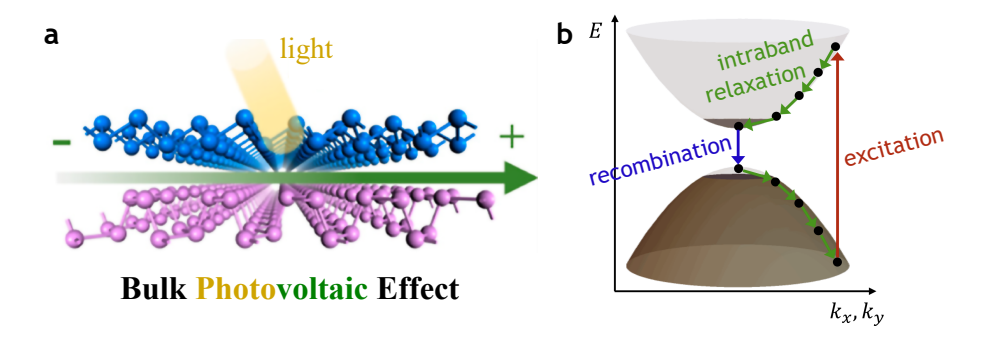


FIG. 4. **Photovoltaic shift current.** (a) Elementary schematic of the shift current, where a dc-current flows in a non-centrosymmetric material under illumination (without external bias). (Image source: Ref. 41.) (b) Various microscopic processes contribute to the shift current. The discussed quantized results relate to the 'excitation' component of the shift current. (Image adapted from Ref. 37.)

freedom in vector bundles [46].⁴ In the interesting cases where the vector bundle is topologically non-trivial (e.g., when it carries a Chern number), a *global* smooth gauge for Bloch states $|u_n(k)\rangle$ over the entire Brillouin zone (BZ) does not exist. This forces geometers to cover BZ with overlapping local neighborhoods \mathcal{U}_{λ} , finding a *local* smooth gauge in each. However, when comparing the gauge on two overlapping neighborhoods, the geometers face a subtle problem: while there is a unique ray $\mathbb{C} \subset \mathcal{H}$ associated with the eigenstate $|u_n(k)\rangle$ at momentum $k \in \mathcal{U}_{\lambda} \cap \mathcal{U}_{\mu}$, this complex ray is not equipped with any canonical choice of basis vector. Therefore, upon comparison, the two geometers find that their basis vectors e_{λ} , e_{μ} are rotated with respect to each other as $e_{\lambda} = g_{\lambda\mu}e_{\mu}$ where $g_{\lambda\mu}(k) \in U(1)$ is called a transition function [Fig. 6(a)]. One can use the transition function to express the difference of the Berry connection in the two bases as $A_{(\lambda)}-A_{(\mu)}=g_{\lambda\mu}^{-1}dg_{\lambda\mu}$ (as expected of a gauge transformation). After taking a derivative, one finds $F_{(\lambda)} = F_{(\nu)}$, i.e., the two geometers agree on the curvature. On triple overlaps, the transition functions are shown to obey so-called 2-cocycle condition $g_{\lambda\mu}g_{\mu\nu}g_{\nu\lambda}=1$ [Fig. 6(b)], which implies a relation to invariants in the second cohomology group $H^2(BZ, \mathbb{Z})$.

To construct a bundle gerbe, we introduce one more level of complexity: we attach a complex ray to all points of every double overlap $\mathcal{U}_{\lambda} \cap \mathcal{U}_{\mu}$. The pair of geometers that meet here agree on their shared choice of the basis vector $e_{\lambda\mu}$ for the rays on this double overlap. Crucially, on the *triple* overlap $k \in \mathcal{U}_{\lambda} \cap \mathcal{U}_{\mu} \cap \mathcal{U}_{\nu}$ every double overlap becomes furnished with its own basis vector, providing us with $(e_{\lambda\mu}, e_{\lambda\nu}, e_{\mu\nu})$. When all three geometers meet, they compare their unit vectors using a generalized transition function $g_{\lambda\mu\nu}(k) \in U(1)$ that relates the *tensor product* $e_{\lambda\mu} \otimes e_{\mu\nu} = g_{\lambda\mu\nu} e_{\lambda\nu}$ [Fig. 6(c)]. One can show that the ordinary (1-form) connections computed from these

three bases obey $A_{(\lambda\mu)}+A_{(\mu\nu)}+A_{(\nu\lambda)}=g_{\lambda\mu\nu}^{-1}dg_{\lambda\mu\nu}$. By taking the derivative of this relation, the corresponding 2-form curvatures obey $F_{(\lambda\mu)}+F_{(\mu\nu)}+F_{(\nu\lambda)}=0$, which allows us to equip each neighborhood with a 2-form potential $\mathcal{B}_{(\lambda)}$ such that $dA_{(\lambda\mu)}=F_{(\lambda\mu)}=\mathcal{B}_{(\mu)}-\mathcal{B}_{(\lambda)}$. Taking a derivative of the last expression and defining the 3-form $\mathcal{H}_{(\lambda)}=d\mathcal{B}_{(\lambda)}$, we find that the geometers agree on the value of $\mathcal{H}_{(\lambda)}=\mathcal{H}_{(\beta)}=\mathcal{H}_{(\gamma)}$. The gauge-dependent object \mathcal{B} is the sought 2-form connection, and the gauge-independent quantity \mathcal{H} is the associated 3-form curvature. The presented construction also generalizes the case of vector bundles in that, on fourfold overlaps, the 3-cocycle condition $g_{\lambda\mu\nu}g_{\lambda\nu\xi}g_{\mu\nu\xi}^{-1}g_{\lambda\mu\xi}^{-1}=1$ holds [Fig. 6(d)], implying a relation to the third cohomology group $H^3(\mathrm{BZ},\mathbb{Z})$.

It may appear mysterious how such a complicated mathematical object may arise in band theory; however, there is a convenient shortcut [49]. To proceed, one needs to identify a triplet of scalar fields $\phi_{1,2,3}$ (two complex and one "pseudoreal") that obey the gauge transformation

$$\phi_1 \mapsto \phi_1 e^{i\chi(k)}, \ \phi_2 \mapsto \phi_2 e^{-i\chi(k)}, \ \text{and} \ \phi_3 \mapsto \phi_3 + \chi(k).$$
 (7)

Then, the Kalb-Ramond field reads

$$\mathcal{B}_{ab}^{nm} \propto \sum_{ijk} \epsilon^{ijk} \phi_i \partial_a \phi_j \partial_b \phi_k, \tag{8}$$

where ϵ^{ijk} is the fully antisymmetric symbol. The field \mathcal{B}^{nm} has the transformation properties expected of a connection 2-form (also called a *tensor connection*). In spinless-PT-symmetric models, two of these fields can be constructed from (energetically isolated) Bloch states $|u_n(k)\rangle$ and $|u_m(k)\rangle$ upon fixing an orbital $|j\rangle$ as $\phi_1(k)=\langle j|u_n(k)\rangle$ (i.e., the orbital-j component of $|u_n\rangle$) and $\phi_2(k)=\langle u_m(k)|j\rangle$ [44]. The remaining field $\phi_3^\chi(k)$ is defined as the line integral of the inter-band connection A_{nm} on a suitably defined path terminating at k.

The three scalar fields as well as the tensor connection \mathcal{B} all change under gauge transformation of the Bloch states; however, the symmetrized derivative

$$\mathcal{H}_{xyz}^{nm} = \partial_x \mathcal{B}_{yz}^{nm} + \partial_y \mathcal{B}_{zx}^{nm} + \partial_z \mathcal{B}_{xy}^{nm}, \tag{9}$$

⁴ In this exposition, I intentionally avoid the language of category theory. For a categorical perspective into higher gauge theory, see Refs. [47] and [48].

⁵ By the 'ray' of the state $|\psi\rangle$ we mean the linear span $[\psi] = \{\lambda | \psi\rangle | \lambda \in \mathbb{C}\}$, which is a linear subspace of the Hilbert space \mathscr{H} .

 $^{^6}$ Unsurprisingly, this invariant is precisely the Chern number. Upon employing Čech cohomology [replacement of n-fold overlaps of neighborhoods by (n-1)-simplices], the Chern number of the vector bundle can be extracted solely from the knowledge of the transition functions $g_{\lambda\mu}$.

⁷ An alternative construction of the fields φ_{1,2,3} entering Eq. (8) was proposed for three-band models with chiral symmetry [49].

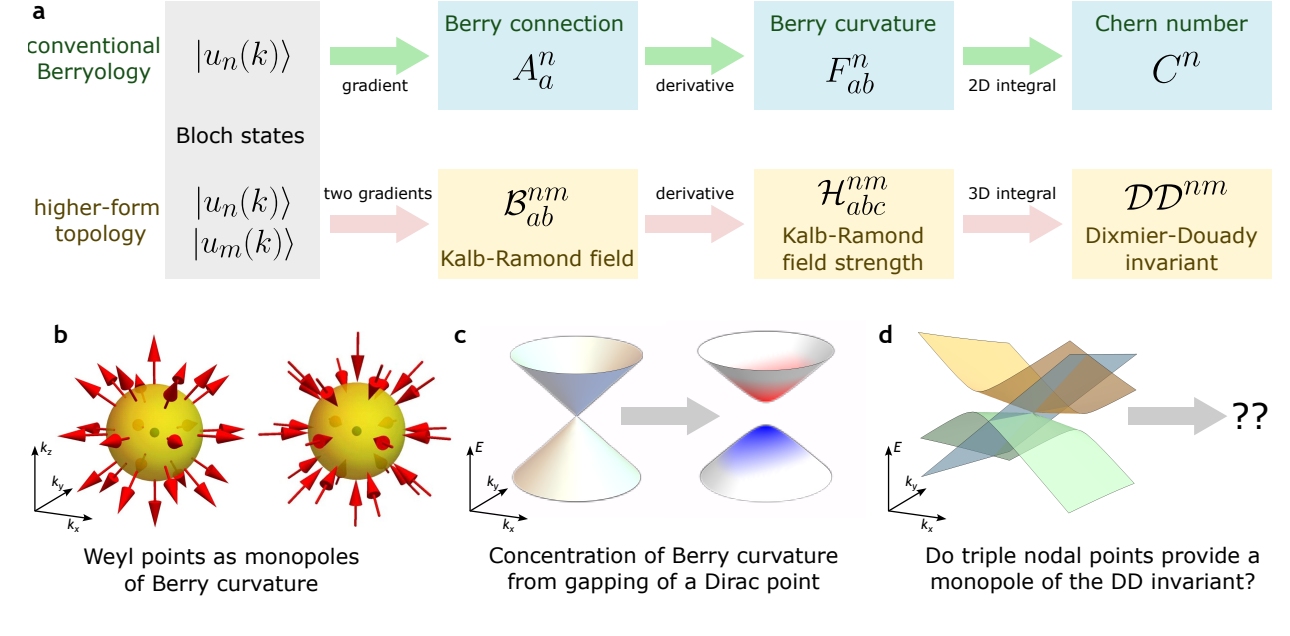


FIG. 5. Comparing Berry quantities against the higher-form topological structures. (a) Flowchart for computing the Chern number vs. the Dixmier-Douady invariant. (b) Weyl points (enclosed dots) in 3D crystals act as sources and drains of a quantum of Berry curvature (red arrows). (c) Opening of an energy gap in Dirac points in 2D crystals generates a large concentration of Berry curvature. (d) What are the analogous three-band objects that acts as monopoles or concentrations of the Kalb-Ramond curvature?

called the *Kalb-Ramond field strength* (or sometimes as *higher Berry curvature*), is a gauge-invariant curvature 3-form. It has been established [44] that, in the presence of PT, the 3-form curvature \mathcal{H}^{nm}_{xyz} can be non-zero only in models with three or more energy bands. Importantly, the integral

$$\mathcal{D}\mathcal{D}^{nm} = -\frac{1}{4\pi^2} \int_{BZ} d^3k \,\mathcal{H}_{xyz}^{nm},\tag{10}$$

which enters the integrated circular shift photoconductivity [Eq. (6)], is an integer called the Dixmier-Douady invariant of the bands $|u_n\rangle$ and $|u_m\rangle$, and it constitutes a higher-cohomology (and thus higher-dimensional) analog of the Chern number. From the experimental vantage point, if the \mathcal{DD} invariant is nonzero, the integrated circular shift photoconductivity changes sign under swapping the pump helicity and is stable to gentle band-structure perturbations that maintain the energy gap. In spinless PT-symmetric systems with non-degenerate bands, every pair of bands n,m is characterized by a \mathcal{DD} invariant (although they are not all independent of each other). In the presence of band degeneracies, quantization is only ensured if one sums contributions over all degenerate bands.

IV. OUTLOOKS FOR FUTURE RESEARCH

The introduction of higher-form topological structures in the description of optical responses invites manifold questions. In particular, while quantum metric and tensor Berry connections have been related to each other [50], a deeper analysis still remains to be conducted. Notably, recall that Weyl points in 3D act as monopole sources of Berry curvature [Fig. 5(b)] and that opening a gap in Dirac points in 2D through symmetry-breaking generates a half-quantum concentration of Berry curvature near the avoided crossing [Fig. 5(c)]. What are the analogous minimal models for solid-state realizations of a 'Kalb-Ramond monopole' (more commonly called a tensor monopole in the literature)? Since a minimum of three bands are necessary to generate the $\mathcal{D}\mathcal{D}$ invariant in PTsymmetric models, it seems natural to start searching for strong concentrations of higher-form curvature (and of an unusually strong circular shift current response) in antiferromagnetic crystals hosting three-fold band degeneracies [Fig. 5(d)]. Such triple nodal points, which have been classified across all magnetic space groups [51], should therefore be revisited from the newly accessed vantage point. Note also that elementary chiral-symmetric models of a tensor monopole have been theoretically described [50] and experimentally simulated in a range of synthetic platforms [52-56], though they do not directly translate to realistic solid-state Hamiltonians without chiral symmetry.

In a similar spirit, higher-fold band degeneracies dubbed multifold fermions [57] could provide means for realizing the tensor monopole in $k \cdot p$ models with four or more energy bands. Such construction has already been pointed out at the theoretical level for the case of the fourfold degenerate spin-3/2 fermions [58]. In this context, note that non-linear photoconductivities of certain multifold fermions have been investigated [59, 60]; however, reports of a quantized shift-current response in these computations are presently missing.

⁸ In the absence of PT symmetry, a two-band system with a single energy gap is already sufficient to introduce the higher-form topology. Namely, the Hopf invariant can be recast as the invariant \mathcal{DD}^{11} of the occupied band [44].

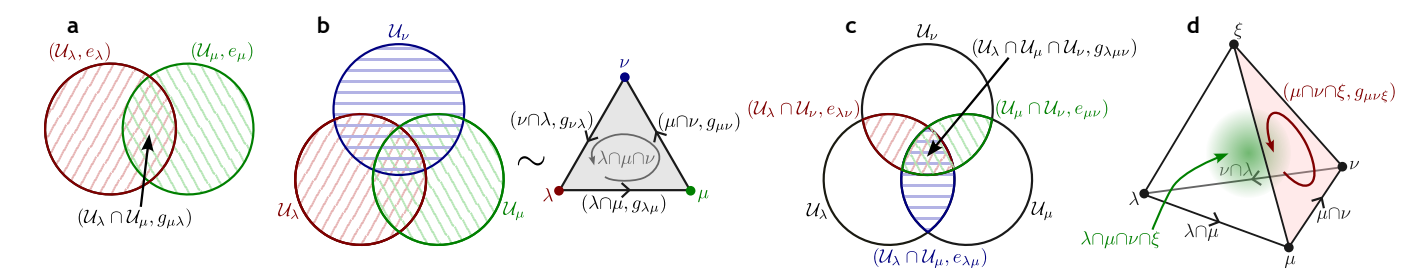


FIG. 6. Vector bundles vs. bundle gerbes. (a) On a vector bundle, one equips local neighborhood \mathcal{U}_{λ} with basis vectors e_{λ} . On double overlaps, the two bases e_{λ} , e_{μ} are related by a transition function $g_{\lambda\mu}$. (b) Representing a triple overlap as a triangle (whose oriented edges are double overlaps, and vertices are the individual neighborhoods), one finds that the three transition functions at the edges obey the 2-cocycle condition. (c) To obtain a bundle gerbe, we equip each double overlap $\mathcal{U}_{\lambda} \cap \mathcal{U}_{\mu}$ with a basis vector $e_{\lambda\mu}$. On triple overlaps, the three basis vectors are related through a generalized transition function $g_{\lambda\mu\nu}$. (d) Representing a fourfold overlap as a tetrahedron, one finds that the four generalized transition functions assigned to the oriented triangular faces obey the 3-cocycle condition.

The principal obstacle in facilitating such endeavors is the lack of a general understanding of the symmetry conditions that admit realizations of the 3-form curvature and of a quantum of the $\mathcal{D}\mathcal{D}$ invariant. In particular, the construction of the Kalb-Ramond field in Eq. (8) has been cleanly formulated only for a narrow range of symmetry settings, such as Hamiltonians with chiral symmetry [50], spinless PT symmetry [44], or both [61]. The existing literature in this direction has not yet clarified how (if at all) one can extend these considerations to other Altland-Zirnbauer symmetry classes, such as those with spinful or spinless time-reversal symmetry, which are ubiquitous in crystals. In fact, even the elementary question of how the 3-form curvature transforms under space group symmetries has not been directly addressed.

It is tempting to consider delicate and multigap topological models as toy laboratories for extending higher-form topology to further symmetry setups. Indeed, while their unstable topology is typically lost upon the inclusion of additional bands, the $\mathcal{D}\mathcal{D}$ invariant can remain well-defined after such a modification and may even enter the response theory, as exemplified by Eq. (6). However, while plentiful examples of unstable topologies are known in spinless-PT-symmetric and time-reversal-breaking models, very few extensions have, to date, been proposed in the presence of additional space group symmetries and in other Altland-Zirnbauer classes. Besides the already mentioned RTP insulators [29], these include Chern dartboard insulators [62, 63], spin Hopf insulators [64], and delicate Wannier insulators [65]. A systematic classification of delicate and multigap topology across a broader range of settings could, potentially, provide a roadmap towards extending the higher-form topological description of energy bands. More broadly, it should also be interesting to consider whether other types of non-linear conductivity could similarly support a deeper and hitherto overlooked topological formulation.

Further opportunities for improvement exist on the computational front. Specifically, any high-throughput search for a solid-state realization of the tensor monopole could be signifi-

cantly accelerated by a reformulation of the curvature in Eq. (9) in a manner that accounts for the topological nature of its integral. Such a formulation is well recognized for the Chern number in 2D by virtue of the Fukui-Hatsugai-Suzuki algorithm [66], which has been recently generalized to the winding number of unitary matrices in 3D [67]. The identification of suitable material candidates would, in turn, open the stage for their ARPES and photoconductivity studies.

It is also natural to wonder if higher-form topology is limited to 'pristine' single-particle Hamiltonians or whether it survives generalization to the 'dirty' cases with disorder and strong correlations. In this respect, it is worth recalling the extension of the Chern number by Niu and Thouless to such a more general scenario by virtue of twisted boundary conditions [68], where the role of momentum is replaced by the twist angles. This idea naturally extends to the $\mathcal{D}\mathcal{D}$ invariant [44], though it remains an open problem to find a concrete variational many-body wave function that realizes a nontrivial value of the invariant. In addition, a connection to strong disorder readily exists through the relation of multi-gap topology to ultra-localized topological insulators [30, 40]. It is interesting to speculate if this relation could be extended towards higherform topology and non-linear responses. Finally, let me point out that the language of higher-form topological structures has, over the past two years, been extended to matrix-product states (i.e., quantum many-body states with short-range entanglement) in 1D [69–72] and even to projected entangled pair states in 2D [73]. In addition, several works have also opened the door to consider realizations of higher-form topology and tensor monopoles in non-Hermitian matter [74, 75].

Overall, the early stage of research into higher-form topology in crystalline matter (alongside the associated questions into quantum geometry and non-linear optics) suggests that impactful contributions can be achieved across all segments of the discovery process, ranging from mathematical characterization and space-group symmetry analysis, through toy models and materials design, to experimental investigations. In concert, these capabilities can deliver definitive tests of quantum-geometry-based bounds and $\mathcal{D}\mathcal{D}$ -quantized shift currents, providing a route toward practical materials with large bulk photovoltaic responses.

⁹ The topology of the last two examples is, in fact, even more subtle, as it is protected by the closing of the Wannier gap rather than of the energy gap.

V. ACKNOWLEDGMENTS

A version of this text has previously appeared as a *Scientific Perspective* in the newsletter of the Swiss MaNEP (Materials with Novel Electronic Properties) network [76]. I would like to thank Frédéric Mila for inviting me to contribute to MaNEP with a short perspective on recent progress in topological band theory. I am further grateful to Aris Alexandradinata, Titus

Neupert, Robert-Jan Slager, and Bohm-Jung Yang for their valuable comments on an early version of this Perspective and to Giandomenico Palumbo for his insightful comments on the recent studies of bundle gerbes in band structures. Finally, I would like to express my special gratitude to Wojciech Jankowski for his critical reading and extensive feedback on the entire text. This work was supported by Starting Grant No. 211310 from the Swiss National Science Foundation.

- J. K. Asbóth, L. Oroszlány, and A. Pályi, A Short Course on Topological Insulators, Lecture Notes in Physics, Vol. 919 (Springer, Cham, 2016).
- [2] D. Xiao, M.-C. Chang, and Q. Niu, Berry phase effects on electronic properties, Rev. Mod. Phys. 82, 1959 (2010).
- [3] M. V. Berry, Quantal phase factors accompanying adiabatic changes, Proc. R. Soc. Lond. A 392, 45 (1984).
- [4] J. P. Provost and G. Vallee, Riemannian structure on manifolds of quantum states, Commun. Math. Phys. 76, 289 (1980).
- [5] P. Zanardi, P. Giorda, and M. Cozzini, Information-Theoretic Differential Geometry of Quantum Phase Transitions, Phys. Rev. Lett. 99, 100603 (2007).
- [6] Y.-Q. Ma, S. Chen, H. Fan, and W.-M. Liu, Abelian and non-Abelian quantum geometric tensor, Phys. Rev. B 81, 245129 (2010).
- [7] J. Yu, C. J. Ciccarino, R. Bianco, I. Errea, P. Narang, and B. A. Bernevig, Non-trivial quantum geometry and the strength of electron-phonon coupling, Nat. Phys. 20, 1262 (2024).
- [8] J. Herzog-Arbeitman, V. Peri, F. Schindler, S. D. Huber, and B. A. Bernevig, Superfluid Weight Bounds from Symmetry and Quantum Geometry in Flat Bands, Phys. Rev. Lett. 128, 087002 (2022).
- [9] P. Törmä, Essay: Where Can Quantum Geometry Lead Us?, Phys. Rev. Lett. 131, 240001 (2023).
- [10] T. Ozawa and B. Mera, Relations between topology and the quantum metric for Chern insulators, Phys. Rev. B 104, 045103 (2021).
- [11] Y. Onishi and L. Fu, Fundamental Bound on Topological Gap, Phys. Rev. X 14, 011052 (2024).
- [12] J. Ahn, G.-Y. Guo, N. Nagaosa, and A. Vishwanath, Riemannian geometry of resonant optical responses, Nat. Phys. 18, 290 (2022).
- [13] B. Ghosh, Y. Onishi, S.-Y. Xu, H. Lin, L. Fu, and A. Bansil, Probing quantum geometry through optical conductivity and magnetic circular dichroism, Sci. Adv. 10, eado1761 (2024).
- [14] M. Kang, S. Kim, Y. Qian, P. M. Neves, L. Ye, J. Jung, D. Puntel, F. Mazzola, S. Fang, C. Jozwiak, A. Bostwick, E. Rotenberg, J. Fuji, I. Vobornik, J.-H. Park, J. G. Checkelsky, B.-J. Yang, and R. Comin, Measurements of the quantum geometric tensor in solids, Nat. Phys. 21, 110 (2025).
- [15] S. Kim, Y. Chung, Y. Qian, S. Park, C. Jozwiak, E. Rotenberg, A. Bostwick, K. S. Kim, and B.-J. Yang, Direct measurement of the quantum metric tensor in solids, Science 388, 1050 (2025).
- [16] S. Gassner and E. J. Mele, Regularized lattice theory for spatially dispersive nonlinear optical conductivities, Phys. Rev. B 108, 085403 (2023).
- [17] A. Avdoshkin, J. Mitscherling, and J. E. Moore, Multistate Geometry of Shift Current and Polarization, Phys. Rev. Lett. 135, 066901 (2025).

- [18] A. Kitaev, Periodic table for topological insulators and superconductors, AIP Conf. Proc. 1134, 22 (2009).
- [19] S. Ryu, A. P. Schnyder, A. Furusaki, and A. W. W. Ludwig, Topological insulators and superconductors: tenfold way and dimensional hierarchy, New J. Phys. 12, 065010 (2010).
- [20] A. Altland and M. R. Zirnbauer, Nonstandard symmetry classes in mesoscopic normal-superconducting hybrid structures, Phys. Rev. B 55, 1142 (1997).
- [21] H. C. Po, A. Vishwanath, and H. Watanabe, Symmetry-based indicators of band topology in the 230 space groups, Nat. Commun. 8, 50 (2017).
- [22] J. Kruthoff, J. de Boer, J. van Wezel, C. L. Kane, and R.-J. Slager, Topological Classification of Crystalline Insulators through Band Structure Combinatorics, Phys. Rev. X 7, 041069 (2017).
- [23] B. Bradlyn, L. Elcoro, J. Cano, M. G. Vergniory, Z. Wang, C. Felser, M. I. Aroyo, and B. A. Bernevig, Topological quantum chemistry, Nature 547, 298 (2017).
- [24] H. C. Po, H. Watanabe, and A. Vishwanath, Fragile Topology and Wannier Obstructions, Phys. Rev. Lett. 121, 126402 (2018).
- [25] J. E. Moore, Y. Ran, and X.-G. Wen, Topological Surface States in Three-Dimensional Magnetic Insulators, Phys. Rev. Lett. 101, 186805 (2008).
- [26] Q. Wu, A. A. Soluyanov, and T. Bzdušek, Non-Abelian band topology in noninteracting metals, Science 365, 1273 (2019).
- [27] A. Bouhon, Q. Wu, R.-J. Slager, H. Weng, O. V. Yazyev, and T. Bzdušek, Non-Abelian reciprocal braiding of Weyl points and its manifestation in ZrTe, Nat. Phys. 16, 1137 (2020).
- [28] B. Jiang, A. Bouhon, Z.-K. Lin, X. Zhou, B. Hou, F. Li, R.-J. Slager, and J.-H. Jiang, Experimental observation of non-Abelian topological acoustic semimetals and their phase transitions, Nat. Phys. 17, 1239 (2021).
- [29] A. Nelson, T. Neupert, T. Bzdušek, and A. Alexandradinata, Multicellularity of Delicate Topological Insulators, Phys. Rev. Lett. 126, 216404 (2021).
- [30] B. Lapierre, T. Neupert, and L. Trifunovic, N-band Hopf insulator, Phys. Rev. Res. 3, 033045 (2021).
- [31] W. J. Jankowski, A. S. Morris, A. Bouhon, F. N. Ünal, and R.-J. Slager, Optical manifestations and bounds of topological Euler class, Phys. Rev. B 111, L081103 (2025).
- [32] H. Lim, S. Kim, and B.-J. Yang, Phys. Rev. B 108, 125101 (2023).
- [33] Z. Davoyan, W. J. Jankowski, A. Bouhon, and R.-J. Slager, Three-dimensional PT-symmetric topological phases with a Pontryagin index, Phys. Rev. B 109, 165125 (2024).
- [34] W. J. Jankowski and R.-J. Slager, Quantized integrated shift effect in multigap topological phases, Phys. Rev. Lett. 133, 186601 (2024).
- [35] A. Alexandradinata, Quantization of intraband and interband Berry phases in the shift current, Phys. Rev. B 110, 075159 (2024).

- [36] W. J. Jankowski, A. S. Morris, Z. Davoyan, A. Bouhon, F. N. Ünal, and R.-J. Slager, Non-Abelian Hopf-Euler insulators, Phys. Rev. B 110, 075135 (2024).
- [37] P. Zhu and A. Alexandradinata, Anomalous shift and optical vorticity in the steady photovoltaic current, Phys. Rev. B 110, 115108 (2024).
- [38] B. I. Sturman, Ballistic and shift currents in the bulk photovoltaic effect theory, Phys.-Uspekhi 63, 407 (2020).
- [39] A. Alexandradinata, A. Nelson, and A. A. Soluyanov, Teleportation of Berry curvature on the surface of a Hopf insulator, Phys. Rev. B 103, 045107 (2021).
- [40] B. Lapierre, L. Trifunovic, T. Neupert, and P. W. Brouwer, Topology of ultra-localized insulators and superconductors (2024), arXiv:2407.07957 [cond-mat.mes-hall].
- [41] J. Xin and Y. Guo, Bulk Photovoltaic Effect in the Elemental Blue Phosphorus-Based Polar Homojunction and Heterojunction, J. Phys. Chem. C 128, 9705 (2024).
- [42] D. Vanderbilt, Berry Phases in Electronic Structure Theory: Electric Polarization, Orbital Magnetization and Topological Insulators (Cambridge University Press, Cambridge, England, 2018).
- [43] J. C. Baez and J. P. Muniain, *Gauge fields, knots and grav-ity*, Knots and Everything, Vol. 4 (World Scientific, Singapore, 1994).
- [44] W. J. Jankowski, R.-J. Slager, and G. Palumbo, Probing Tensor Monopoles and Gerbe Invariants in Three-Dimensional Topological Matter (2025), arXiv:2507.22116 [cond-mat.mes-hall].
- [45] M. Kalb and P. Ramond, Classical direct interstring action, Phys. Rev. D 9, 2273 (1974).
- [46] M. K. Murray, Bundle gerbes, J. Lond. Math. Soc. 54, 403 (1996).
- [47] J. C. Baez and U. Schreiber, Higher Gauge Theory, in *Contemporary Mathematics*, Vol. 431, edited by A. Davydov *et al.* (American Mathematical Society, Providence, RI, 2007) pp. 7–30, arXiv:math/0511710.
- [48] L. Borsten, M. J. Farahani, B. Jurčo, H. Kim, J. Nárožný, D. Rist, C. Saemann, and M. Wolf, Higher Gauge Theory, in *Encyclope-dia of Mathematical Physics (Second Edition)*, edited by R. Szabo and M. Bojowald (Academic Press, Oxford, 2025) second edition ed., pp. 159–185.
- [49] G. Palumbo and N. Goldman, Tensor Berry connections and their topological invariants, Phys. Rev. B 99, 045154 (2019).
- [50] G. Palumbo and N. Goldman, Revealing Tensor Monopoles through Quantum-Metric Measurements, Phys. Rev. Lett. 121, 170401 (2018).
- [51] P. M. Lenggenhager, X. Liu, T. Neupert, and T. Bzdušek, Triple nodal points characterized by their nodal-line structure in all magnetic space groups, Phys. Rev. B 106, 085128 (2022).
- [52] X. Tan, D.-W. Zhang, W. Zheng, X. Yang, S. Song, Z. Han, Y. Dong, Z. Wang, D. Lan, H. Yan, S.-L. Zhu, and Y. Yu, Experimental Observation of Tensor Monopoles with a Superconducting Qudit, Phys. Rev. Lett. 126, 017702 (2021).
- [53] H. Weisbrich, M. Bestler, and W. Belzig, Tensor Monopoles in superconducting systems, Quantum 5, 601 (2021).
- [54] M. Chen, C. Li, G. Palumbo, Y.-Q. Zhu, N. Goldman, and P. Cappellaro, A synthetic monopole source of Kalb-Ramond field in diamond, Science 375, 1017 (2022).
- [55] Y. Zhang, Y.-Q. Zhu, J. Xu, W. Zheng, D. Lan, G. Palumbo, N. Goldman, S.-L. Zhu, X. Tan, Z. Wang, and Y. Yu, Exploring parity magnetic effects through quantum simulation with superconducting qubits, Phys. Rev. Appl. 21, 034052 (2024).

- [56] Q. Mo, S. Liang, C. Lu, J. Zhu, and S. Zhang, Tensor-Monopole-Induced Topological Boundary Effects in Four-Dimensional Acoustic Metamaterials, Phys. Rev. Lett. 134, 186601 (2025).
- [57] B. Bradlyn, J. Cano, Z. Wang, M. G. Vergniory, C. Felser, R. J. Cava, and B. A. Bernevig, Beyond Dirac and Weyl fermions: Unconventional quasiparticles in conventional crystals, Science 353, aaf5037 (2016).
- [58] Y.-Q. Zhu, N. Goldman, and G. Palumbo, Four-dimensional semimetals with tensor monopoles: From surface states to topological responses, Phys. Rev. B 102, 081109 (2020).
- [59] Z. Ni, B. Xu, M.-A. Sánchez-Martínez, Y. Zhang, K. Manna, C. Bernhard, J. W. F. Venderbos, F. de Juan, A. G. Felser, C. Grushin, and L. Wu, Linear and nonlinear optical responses in the chiral multifold semimetal RhSi, npj Quantum Mater. 5, 96 (2020).
- [60] H.-C. Hsu, J.-S. You, J. Ahn, and G.-Y. Guo, Nonlinear photoconductivities and quantum geometry of chiral multifold fermions, Phys. Rev. B 107, 155434 (2023).
- [61] G. Palumbo, Non-Abelian Tensor Berry Connections in Multiband Topological Systems, Phys. Rev. Lett. 126, 246801 (2021).
- [62] P. W. Brouwer and V. Dwivedi, Homotopic classification of band structures: Stable, fragile, delicate, and stable representationprotected topology, Phys. Rev. B 108, 155137 (2023).
- [63] Y.-C. Chen, Y.-P. Lin, and Y.-J. Kao, Chern dartboard insulator: sub-Brillouin zone topology and skyrmion multipoles, Commun. Phys. 7, 32 (2024).
- [64] P. Zhu, A. Alexandradinata, and T. L. Hughes, Z_2 spin Hopf insulator: Helical hinge states and returning Thouless pump, Phys. Rev. B 107, 115159 (2023).
- [65] Z. Guba, A. Alexandradinata, and T. Bzdušek, Delicate Wannier insulators (2025), arXiv:2506.05179 [cond-mat.mes-hall].
- [66] T. Fukui, Y. Hatsugai, and H. Suzuki, Chern Numbers in Discretized Brillouin Zone: Efficient Method of Computing (Spin) Hall Conductances, J. Phys. Soc. Jpn. 74, 1674 (2005).
- [67] K. Shiozaki, A discrete formulation for three-dimensional winding number (2024), arXiv:2403.05291 [cond-mat.mes-hall].
- [68] Q. Niu and D. J. Thouless, Quantised adiabatic charge transport in the presence of substrate disorder and many-body interaction, J. Phys. A 17, 2453 (1984).
- [69] S. Ohyama, Y. Terashima, and K. Shiozaki, Discrete higher Berry phases and matrix product states, Phys. Rev. B 110, 035114 (2024).
- [70] K. Shiozaki, N. Heinsdorf, and S. Ohyama, Higher Berry curvature from matrix product states, Phys. Rev. B 112, 035154 (2025).
- [71] O. E. Sommer, X. Wen, and A. Vishwanath, Higher Berry Curvature from the Wave Function. I. Schmidt Decomposition and Matrix Product States, Phys. Rev. Lett. 134, 146601 (2025).
- [72] S. Ohyama and S. Ryu, Higher Berry connection for matrix product states, Phys. Rev. B 111, 035121 (2025).
- [73] S. Ohyama and S. Ryu, Higher Berry phase from projected entangled pair states in (2 + 1) dimensions, Phys. Rev. B 111, 045112 (2025).
- [74] Y.-Q. Zhu, W. Zheng, S.-L. Zhu, and G. Palumbo, Band topology of pseudo-Hermitian phases through tensor Berry connections and quantum metric, Phys. Rev. B 104, 205103 (2021).
- [75] S.-B. Yang, P.-R. Han, W. Ning, F. Wu, Z.-B. Yang, and S.-B. Zheng, An exceptional surface and its topology (2025), arXiv:2501.04317 [quant-ph].
- [76] T. Bzdušek, From quantum geometry to non-linear optics: recent advances in topological band theory, MaNEP Newsletter 49 (2025).